

First In Situ Evidence for Coexisting Submeter Temperature and Humidity Sheets in the Lower Free Troposphere*

ANDREAS MUSCHINSKI AND CHRISTIAN WODE

Institut für Meteorologie und Klimatologie, Universität Hannover, Hannover, Germany

(Manuscript received 30 September 1996, in final form 16 December 1997)

ABSTRACT

In recent years, temperature “sheets” with thicknesses on the order of 1 m have been observed with high-resolution radiosondes throughout the stably stratified atmosphere, suggesting that they give rise to a major part of the well-known near-zenith aspect sensitivity of VHF radar echo intensities. It has been presumed but as yet not directly observed that these temperature sheets are accompanied by humidity sheets. In this paper, observations using the new helicopter-borne in situ turbulence measurement system HELIPOD are presented and discussed. For the first time it has been possible to observe in situ coexisting atmospheric temperature and humidity sheets with thicknesses down to a few decimeters and with temperature gradients of up to 17Γ , where Γ denotes the adiabatic lapse rate. Moreover, the first directly observed tropospheric temperature, humidity, and wind velocity profiles of a turbulent layer with a thickness of less than 10 m confined between two submeter sheets are presented. Simple theoretical reasoning leads to a lower limit for the sheet thicknesses: regardless of whether they are the remnants of Kelvin–Helmholtz instability or attributed to viscosity/thermal-conduction waves, it should amount (apart from a numerical factor) to the square root of the product of molecular kinematic viscosity and a timescale that characterizes the age of a laminar sheet, the lifetime of a Kelvin–Helmholtz billow, or the period of a primary gravity wave.

1. Introduction

One of the most challenging problems in meteorology and fluid dynamics has been to understand the interaction between wavy motion and turbulent motion in stably stratified flows. Since the discovery of very thin steplike structures in the ocean (Woods 1968), in lakes (Imberger and Ivey 1991), in the atmospheric boundary layer (Gossard et al. 1985), and in the free atmosphere (Dalaudier et al. 1994), things have become even more complicated. These “sheets,” which in the atmosphere have thicknesses on the order of a few meters or even less, appear to be ubiquitous in the case of stable “background” stratification.

Two sorts of models have been suggested to explain the physical nature of the sheets. According to the “sheet and layer models” (e.g., Woods 1969; Posmentier 1977; Gossard et al. 1985; Woodman and Chu 1989), the sheets are accompanied by thin turbulent layers and are both possibly the result of Kelvin–Helmholtz

instability (KHI). KHI is a common phenomenon in stratified shear flows, and it has been observed in the ocean (Woods 1968), in the atmospheric boundary layer (Gossard et al. 1970; Atlas et al. 1970; Gossard et al. 1971; Gossard et al. 1973; Metcalf and Atlas 1973; Eaton et al. 1995), and in the free atmosphere (Hicks and Angell 1968; Browning and Watkins 1970; Klostermeyer and Ruster 1980; Chilson et al. 1997). See also the review article by Fritts and Rastogi (1985).

Other researchers suggest the alternative explanation that “dissipative waves,” “viscosity waves,” or “thermal conduction waves” (Pitteway and Hines 1963; Hooke and Jones 1986; Hocking et al. 1991) could play an important role in the formation of sheets. Those waves are modes of gravity waves with short vertical wavelengths, being strongly damped by the molecular viscosity (Hocking et al. 1991) or by an eddy viscosity (Hooke and Jones 1986). Hocking et al. (1991), Dalaudier et al. (1994), and Luce et al. (1995) suggest that the sheets could be the reason of a dominating part of the aspect sensitivity of VHF radar echo intensities at near-vertical beam directions (Röttger and Liu 1978; Gage and Green 1978). The effect of thin refractive-index laminae on the VHF-echo aspect sensitivity was theoretically investigated by Doviak and Zrnić (1984). Recently, Muschinski (1996a) has shown that systematically tilted thin aspect-sensitive layers associated with Kelvin–Helmholtz billows could also give rise to a significant contribution to the well-known downward bias

* This paper is dedicated to Professor Rainer Roth on the occasion of his 65th birthday.

Corresponding author address: Dr. Andreas Muschinski, CIRES, University of Colorado, and NOAA/Environmental Technology Laboratory, 325 Broadway, R/E/ET4, Boulder, CO 80303.
E-mail: amuschinski@etl.noaa.gov

(Nastrom et al. 1990) of vertical velocities observed with vertically pointing VHF radars.

Hence, high-resolution in situ measurements of the atmospheric temperature and humidity fine structure are important for a more complete understanding of clear-air radar data as well as of the corresponding atmospheric structures and processes.

Gossard et al. (1985) report on coexisting temperature and humidity sheets observed in the stably stratified boundary layer. Although their temperature and humidity data have possibly a sufficiently high resolution (see their Fig. 5), Gossard et al. (1985) concentrate in their paper on vertical profiles of the turbulence structure parameters and do not explicitly consider the profiles with respect to length scales down to 1 m. Luce et al. (1995) expect that also in the free atmosphere there is generally a coexistence of meter-scale temperature sheets and humidity sheets. The vertical resolution of their humidity profiles, however, was not sufficient to prove this hypothesis for vertical scales on the order of 1 m.

We do not know of any observations that would provide in situ evidence for coexisting temperature and humidity sheets on the submeter scale.

The objective of the present paper is to test the hypothesis of coexisting thin temperature and humidity sheets in the free atmosphere by considering high-resolution temperature and humidity profiles measured during the first field operation of the new helicopter-borne multisensor instrument HELIPOD. The paper is organized as follows. Some technical details of HELIPOD are presented in section 2. Section 3 presents the experimental setup and the meteorological and topographical conditions during the HELIPOD experiment on 13 October 1995, which was carried out above the Arctic sea ice. In section 4, observational evidence of coexisting lower-tropospheric temperature and humidity sheets on the submeter scale is shown. The results are discussed in section 5. Summary and conclusions are given in section 6.

2. The helicopter-borne meteorological sensor system HELIPOD

a. Overview and background

For in situ turbulence measurements within the atmospheric boundary layer, generally airplane-based measurement systems are used. Due to logistical, technical, or safety reasons, however, the operation of conventional airplanes often is strongly restricted, sometimes even impossible. In many of those cases helicopters provide a much better suited operation platform. Vörsmann (1990) and Büchler (1993) showed that nowadays the usage of a helicopter-borne sensor system should be possible without unacceptable distortion of the atmospheric turbulence signals through the helicopter's downwash eddies.

The high-resolution meteorological turbulence measurement system HELIPOD is a unique answer to this technical challenge. The system consists of an autonomous container, about 5 m long and 250 kg in weight, which is constructed to be towed with a true airspeed of approximately 40 m s^{-1} on a 15-m-long rope below several kinds of helicopters (Fig. 1). The system can work completely stand alone; however, external system controlling and real-time data preview from inside the helicopter usually is performed, too (Fig. 1, dashed box).

After some former similar ideas (see, e.g., Blanc et al. 1989), HELIPOD is to our knowledge the first and only system that unifies the aerodynamical and logistical advantages of a helicopter as towing aircraft with highly sophisticated meteorological, navigational, and technical sensor equipment. The system allows high-resolution in situ measurements of turbulent fluxes of mass, momentum, sensible heat, and moisture quantities to be made; and it is specially suited for ship-based polar and midocean operation concerning various aspects of meteorological, oceanographical, and hydrological research. HELIPOD has been constructed by the German company "Aerodata Flugmesstechnik GmbH." The authors and several other institutes of different German universities and research establishments contributed scientifically.

The data investigated in this paper were measured with HELIPOD during the recent Arctic campaign ARK-XI/2 of the German polar research vessel *Polarstern*, which took place from 22 September to 29 October 1995 under the motto "autumn in the Greenland Sea" (Krause 1996). The HELIPOD operations during this *Polarstern* campaign were part of the international Arctic Climate System Study (ACSYS; WCRP-72 1992, WCRP-85 1994). The *Polarstern* cruise ARK-XI/2 was one of the first scientific HELIPOD campaigns and the first time at all that HELIPOD was successfully operated from on board a ship. Details on the HELIPOD operation during this campaign are given by Wode and Wamser (1996).

b. Sensor equipment

HELIPOD's meteorological sensor equipment comprises a five-hole probe for static pressure and wind measurements (sampling frequency 100 Hz), two temperature sensors with different response times (100 and 20 Hz), an independent humidity measuring chamber containing a humicap (a capacitive humidity sensor; 20 Hz), a dewpoint mirror (20 Hz), and a Lyman- α hygrometer (100 Hz) as well as an additional temperature (20 Hz) and flow sensor (20 Hz) within the chamber, and finally a radiation thermometer (100 Hz) for surface temperature measurements. The different sensor components of the temperature and humidity subsystems each have a different response time and drift behavior,

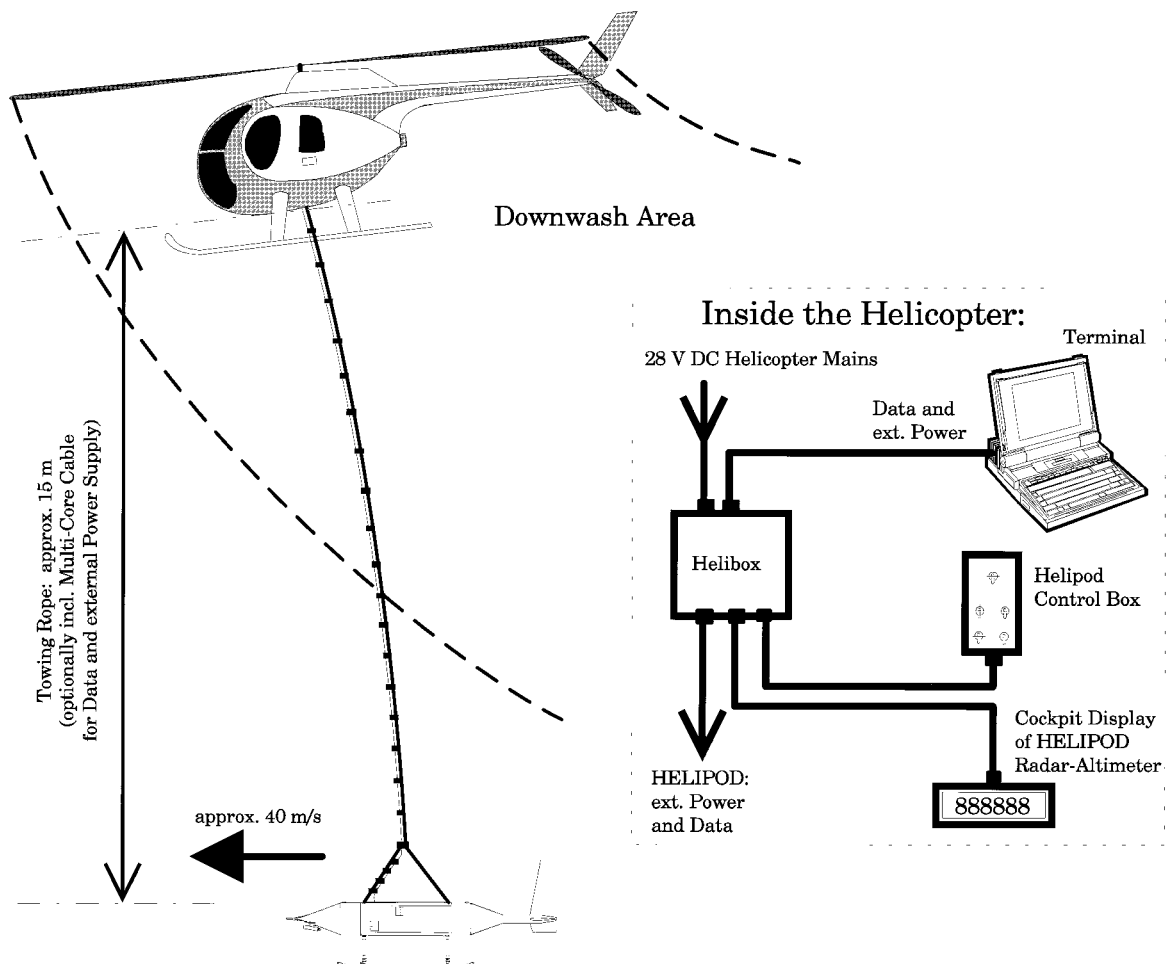


FIG. 1. In-flight system sketch of the helicopter-borne meteorological turbulence measurement system HELIPOD. The sensor container is developed to be towed on a 15-m-long rope with a true airspeed of approximately 40 m s^{-1} . The system can be operated by any helicopter equipped with a cargo hook. The dashed box shows the optional arrangement of control devices inside the helicopter.

and a highly elaborated complementary Kalman filtering algorithm is used to provide temperature and humidity data, which are both sampled with high frequency and are free of long-term drift. These complementary filtering procedures are one of HELIPOD's most important parts within the real-time data processing and storing. An additional improvement is that all 100-Hz meteorological data are internally generated as 10-value averages, being calculated on-line from a 1000-Hz oversampling. This technique acts as an important kind of analogous filter, as it removes all frequencies between HELIPOD's Nyquist frequency (50 Hz) and an internal Nyquist frequency of 500 Hz. As a side effect, this method helps to reduce the digitalization error of the 100-Hz sensors by a factor of about 3.

HELIPOD's navigation system also comprises sensors with different response times and long-term stabilities: a static and a radar altimeter (100 Hz each), an inertial navigation system (INS; 100 Hz), and two different geostationary positioning systems (GPS) (1 Hz),

which together do not only provide the position, but also the attitude of HELIPOD. The GPS navigation acts again as a drift-free support for the INS data: all navigation raw data are complementarily combined by Kalman filter software, which outputs high-frequency, high-precision, and drift-free navigation. In the case that additional information from a ground-based GPS station is available, HELIPOD's navigation can also operate with differential GPS accuracy. This feature is the only one that up to now requires off-line data postprocessing.

Combining all these features, HELIPOD's sensor system has proved to provide accuracies of the wind vector between 0.01 and 0.1 m s^{-1} , of air temperature between 0.01 and 0.05 K , and of specific humidity between 0.001 and 0.01 g kg^{-1} .

The data preprocessing within HELIPOD is done in real time simultaneously by different transputers. The final data storing is real-time controlled by the OS9-VC6 main computer. All meteorological and navigational raw data as well as technical system parameters

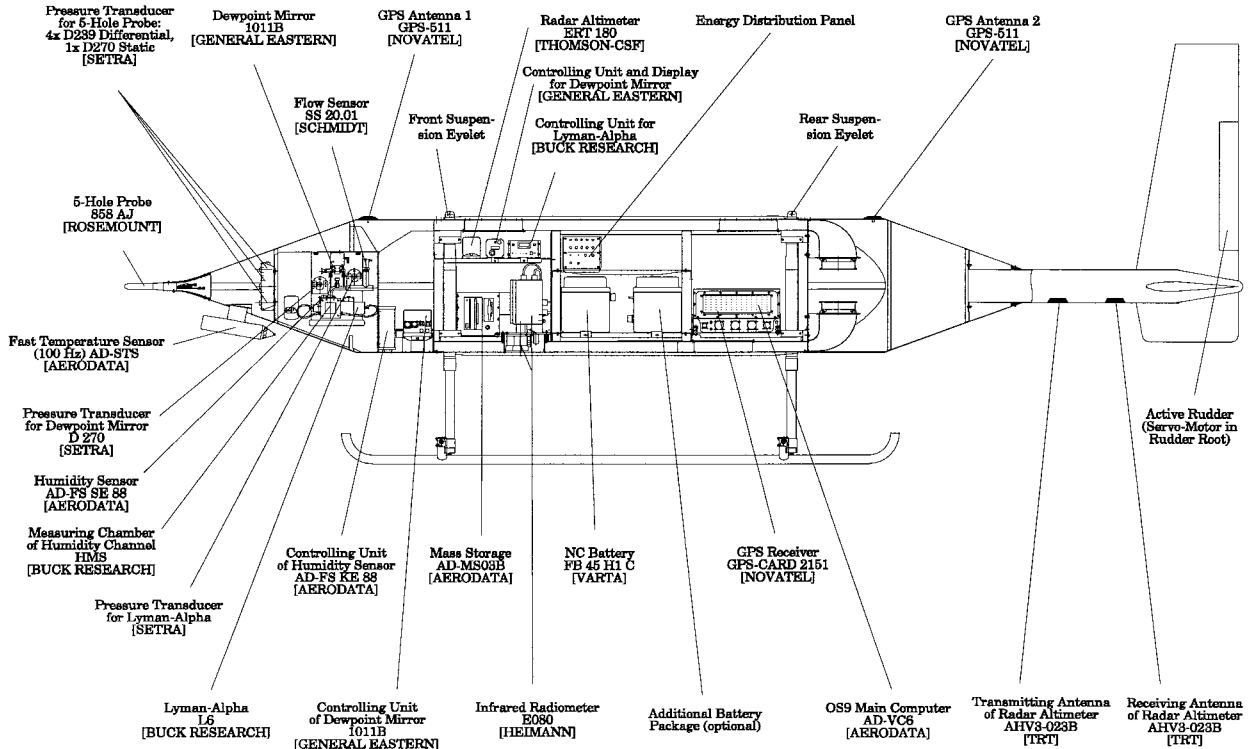


FIG. 2. Sensor components and their arrangement inside HELIPOD. The total length of the HELIPOD system is 5 m, the total weight of all components is 288 kg.

and on-line calculated secondary quantities are recorded in up to 160 channels on magneto-optical disks with a recording capacity of 300 MB on each side, corresponding to about 3-h or 430-km flight pathlength. A special software package allows simultaneously an on-line display of arbitrary data channels on a laptop computer inside the helicopter as well as an in-flight calibration of different sensors.

A longitudinal section of the system's body showing the arrangement of the sensors and technical components inside HELIPOD is shown in Fig. 2. A more comprehensive presentation of the system is given, for example, by Wode and Roth (1996), Wode et al. (1996), and Schürmann and Wode (1996).

c. Off-line data evaluation

The off-line conditioning and processing of the collected data, which usually starts with plausibility checks, elimination of outliers and trends, correction of potential data losses and resulting data gaps, interactive decomposing of longer time series into shorter legs, etc., can be done conveniently with an additional software package, which provides some useful features for efficient, comfortable, and fast data processing. This software tool has been developed using the fourth-generation programming language PV-WAVE. It is run usually on a SUN Sparc 10 workstation, which can be operated either

within a network or can stand alone during field campaigns.

3. Experimental setup, meteorological, and topographical conditions during the experiment on 13 October 1995

On 13 October 1995, *Polarstern* stopped over at 74.98°N, 13.58°W amidst an extended area of nearly homogeneously snow-covered sea ice. (As the East Greenland Current discharges sea ice from the Arctic Basin southward into the warmer parts of the Greenland Sea and the Strait of Denmark, this area is usually covered relatively densely with Arctic sea ice.) The HELIPOD system took off on this day at 1415 UTC and returned back onboard the *Polarstern* at 1623 UTC. The location of the experimental area is shown in Fig. 3.

The weather during this day was fine: The pressure was about 1017 hPa, there were neither low- nor medium-level clouds, not more than one-eighth of cirrocumulus and cirrostratus clouds, ceiling and visibility were unlimited, and the 10-m wind was weak to moderate from 230°. The average wind speed at 10 m AGL (above ground level) amounted to about 6 m s⁻¹, the air temperature near the surface was about -10.8°C, and the dewpoint was about -13°C. The atmosphere was nearly isothermal within the boundary layer, which extended up to about 75 m AGL, and slightly stably

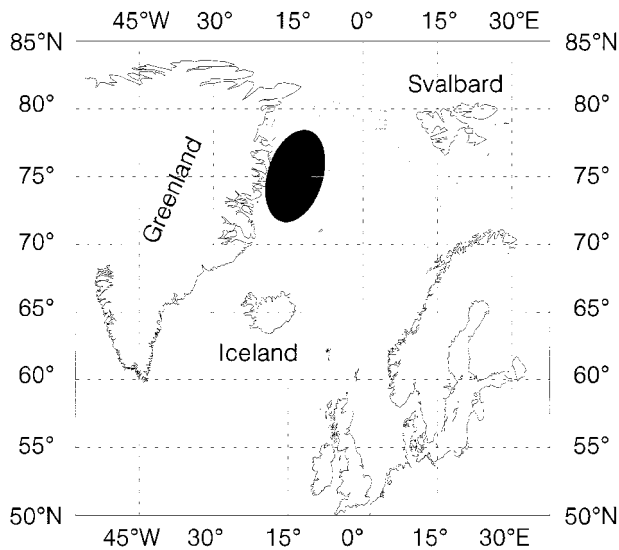


FIG. 3. The operation area during the *Polarstern* cruise ARK-XI/2 in autumn 1995. *Polarstern* left Tromsø, Norway, on 22 September 1995 and reached Bremerhaven, Germany, on 29 October 1995 (gray track). The HELIPOD flight was made on 13 October 1995 between 1415 UTC and 1623 UTC at about 75°N, 13°W (black “+”) in the main working area (black spot) amidst the East Greenland current.

stratified above the inversion. On the synoptic scale, the fine weather was caused by a quasi-stationary high pressure area above central Greenland, the core sea level pressure of which increased from about 1017 hPa on 12 October to 1024 hPa on 14 October 1995. The meteorological situation thus did not change significantly during that day—giving rise to a substantial subsidence, which could clearly be detected by intercomparison of the altitudes of some inversions in the free troposphere within the different HELIPOD soundings.

Originally, the objective of this HELIPOD flight was to investigate the lowest decameters of the atmospheric boundary layer. For this purpose, a two-dimensional flight pattern was used (Fig. 4b), which was orientated within a vertical plane parallel to the 10-m mean wind direction. The flight pattern consisted mainly of seven horizontal legs with a length of about 22 km each, flown in ascending order in (nearly logarithmically spaced) heights at 8, 14, 23, 30, 50, 80, and 130 m AGL. Before the beginning and after the end of the horizontal legs, two additional “double sawtooth” patterns were flown along the same track, consisting of two upward and downward soundings each, in order to monitor the vertical atmospheric structure and its change with time during the flight mission. The true airspeed of the helicopter was maintained at 40 m s^{-1} throughout the whole flight; and the climbing and descending rates during the sawtooth soundings were $\pm 5 \text{ m s}^{-1}$, respectively.

In this paper, exemplarily only data from three of the eight legs of the sawtooth soundings are discussed. (Increasing with time, the single legs of the soundings are denoted with S1 to S8; they are easy to identify in the

time series plot of the barometric height of HELIPOD; see Fig. 4a.) Between the two groups of soundings, a period of 5086 s (about 1 h 25 min) passed during which the seven horizontal legs were flown. In the following, we refer to the soundings S1, S2, and S7 (see Fig. 4a, hatched areas).

4. Temperature and humidity sheets and layers— Observational results

Figures 5a–c show a close-up of a group of temperature sheets and Figs. 5d–f show humidity sheets observed during S1. The altitude range between ground level and about 720 m AGL is depicted in Figs. 5a and 5d. Figures 5b and 5e cover the altitude range between 400 m and 500 m AGL, and Figs. 5c and 5f are an enlargement of the altitude range between 410 m and 430 m AGL. Although the temperature ranges only within the interval between -3.85°C and -3.65°C , there is obviously a well-defined fine structure in the temperature profile. Slightly below 418 m AGL, T increases by 0.04 K within about 30 cm. At 421 m AGL, there is an increase of T by about 0.09 K within less than 40 cm, and a third temperature step can be identified at 425 m AGL, where T increases by 0.08 K within about 40 cm. That is, within an altitude range of 7 m, the temperature increases not continuously but in three well-defined steps of 0.1 K or less each. The standard deviation of the submeter variability of the vertical temperature profile is on the order of 0.01 K within the 20-m interval shown in Fig. 5c, with the exception of the altitude range between the second step at 421 m AGL and the third step at 425 m AGL. In this layer, the temperature is more irregular and exhibits a peak-to-peak variability of about 0.05 K. The temperature gradient across the sheet at 421 m AGL is about 0.3 K per 1.8 m or about 17Γ , which is about the same as the largest temperature gradient that has been reported up to now (Dalaudier et al. 1994). Here, $\Gamma = 9.8 \times 10^{-3} \text{ K m}^{-1}$ denotes the adiabatic lapse rate. Note that the temperature gradient within each of the two “subsheets” of the sheet at 425 m AGL is nearly equal to that determined for the sheet at 421 m AGL.

In the temperature profile shown in Fig. 5b, there are a number of mostly positive temperature “spikes” in the altitude range between 435 m AGL and 465 m AGL, which have an amplitude of 0.05 K and an apparent vertical extent of 1 m or less. There is also a negative spike at 497 m AGL. Since those spikes do not have any counterparts in the humidity profile, we presume that they are artifacts, maybe due to intermittent electronic interference or due to small particles in the air that hit the extremely thin wire.

Figure 6 shows the vertical profiles of (a) the temperature, (b) the specific humidity, (c) the zonal wind velocity, and (d) the meridional wind velocity. Within the 20-m-interval under consideration, the specific hu-

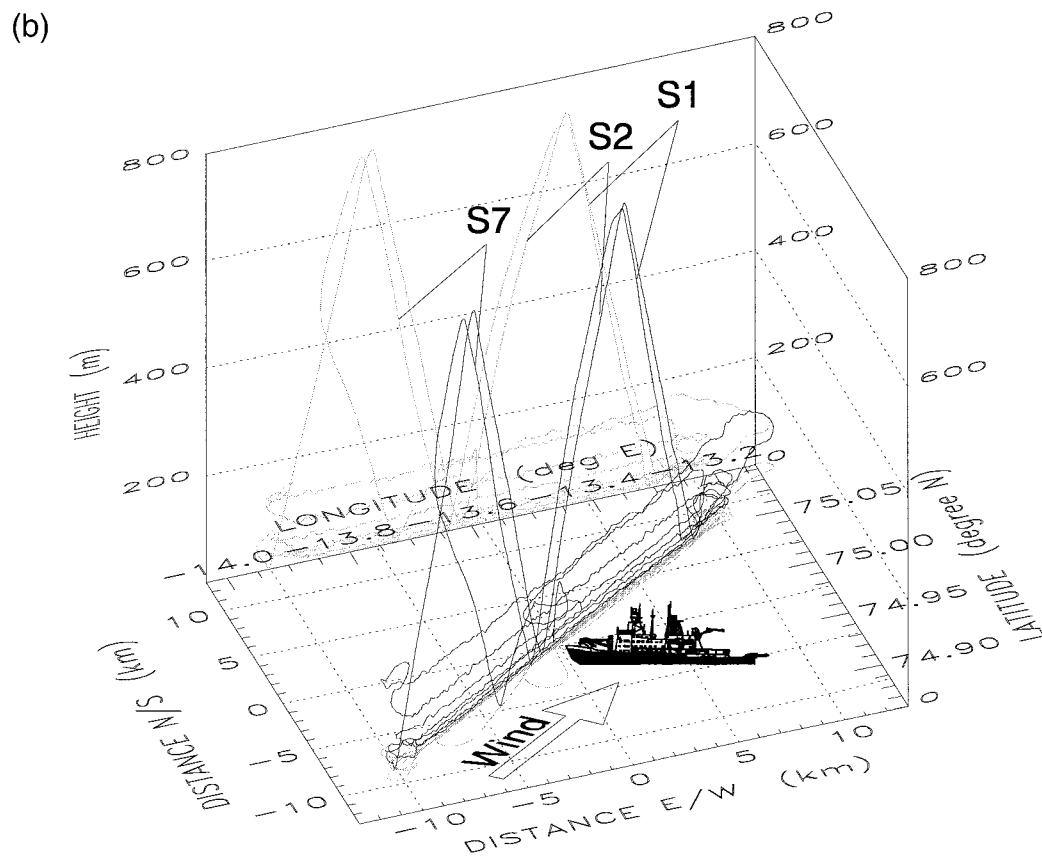
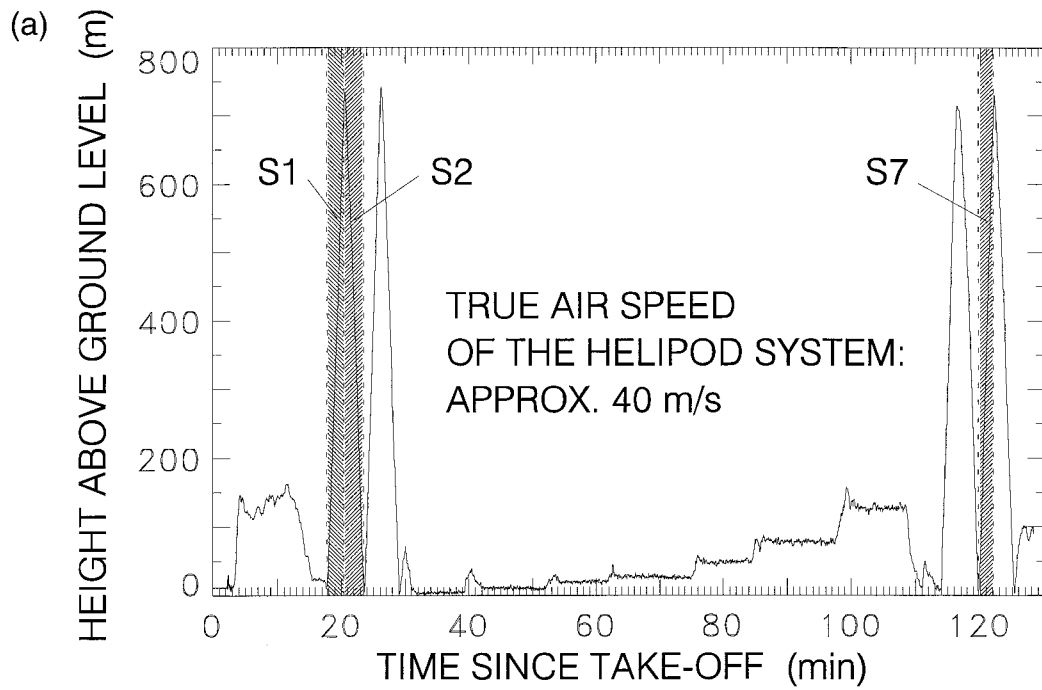


FIG. 4. Three-dimensional flight track (b) and corresponding time series of HELIPOD's altitude (a) on 13 October 1995. In this paper, only data of the sounding legs S1, S2, and S7 are discussed (hatched sections).

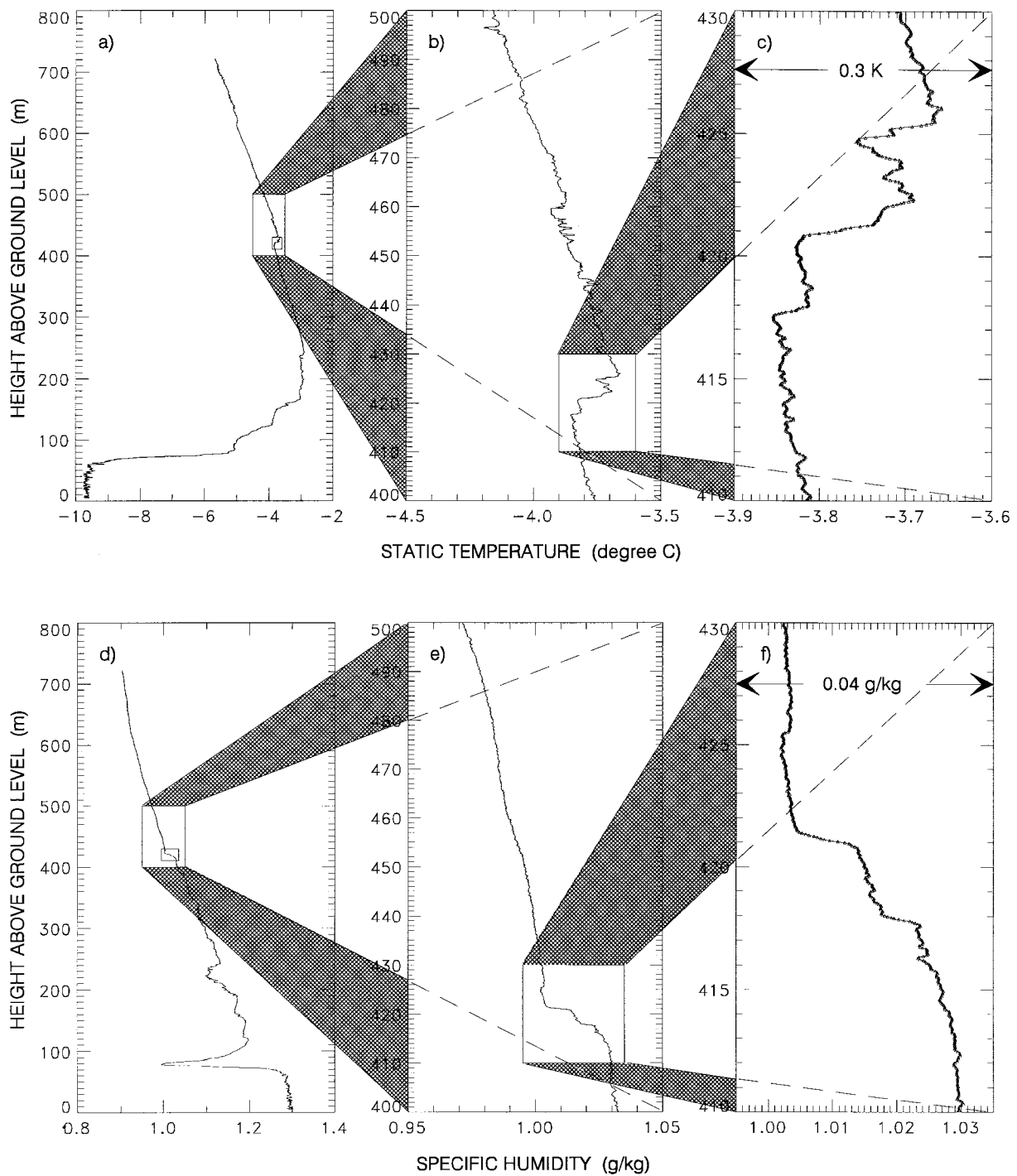


FIG. 5. Close-up of a group of submeter temperature (a)–(c) and humidity sheets (d)–(f), respectively, observed during leg S1. The sheets, corresponding to a strong vertical temperature gradient, can be clearly detected between 417 m and 426 m AGL.

midity q ranges between 1.002×10^{-3} and 1.030×10^{-3} , the zonal wind u between 6.5 m s^{-1} and 7.3 m s^{-1} , and the meridional wind v between -0.1 m s^{-1} and 0.3 m s^{-1} . At the altitudes of the temperature sheets, there are also sudden changes in the specific humidity (see Figs. 6a and 6b). At 418 m AGL, q decreases from

1.023×10^{-3} to 1.018×10^{-3} , at 421 m AGL, q decreases from 1.013×10^{-3} to 1.005×10^{-3} . Between 425 m and 426 m AGL, however, there is an *increase* from 1.002×10^{-3} to 1.003×10^{-3} .

One of the most beautiful examples of coexisting temperature and humidity sheets that we found in our da-

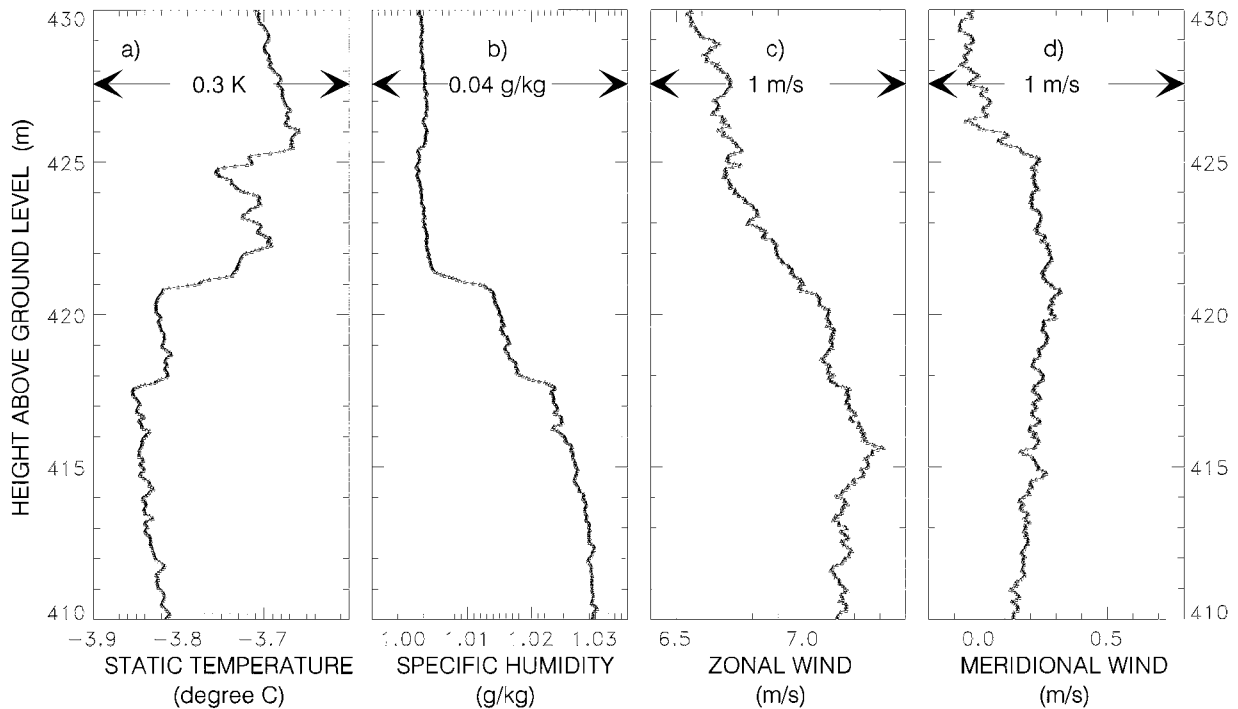


FIG. 6. Vertical profiles of four quantities observed during leg S1 when traversing the group of sheets in the altitude interval between 410 m and 430 m AGL: (a) temperature, (b) specific humidity, (c) zonal wind, and (d) meridional wind.

taset is shown in Fig. 7. The data are from S7. Between 324 m AGL and 330 m AGL, that is within an altitude interval of 6 m, the temperature increases from -3.26°C to -2.79°C , that is by 0.47°C . In the same altitude range, q increases from 0.75×10^{-3} to 0.92×10^{-3} . This is a relative increase by about 25%. More than half of this change in q occurs within less than 1 m, that is, between 327 m AGL and 328 m AGL. There is also a significant change in the wind direction; see Figs. 7c and 7d. While the zonal wind does not vary considerably across the sheet, the meridional wind increases by 0.32 m s^{-1} within the 2-m interval between 327 m AGL and 329 m AGL. This corresponds to a wind shear of $160 \text{ m s}^{-1} \text{ km}^{-1}$.

Figure 8 shows an 8-m-thick turbulent layer embedded between two sheets at 199 m AGL and at 207 m AGL, respectively. The layer was observed during S2. Note the steepening of the temperature gradient at the lower and upper boundary of the turbulent layer. Our observational results are very similar to Dalaudier et al.'s (1994) observations of a turbulent layer at an altitude of almost 12 km (see "sheet" b in their Fig. 1). Their layer was also about 8 m thick, and the temperature increase across their layer was 0.39 K. The temperature increase in Fig. 8 is about 0.30 K.

5. Discussion

a. Observed properties of the sheets and layers

Before discussing in more detail the physical properties of the observed structures, the following summarizes our observations.

Observations were presented for three cases of atmospheric fine structure: (i) a group of three submeter sheets within an altitude interval of about 8 m (Fig. 6); (ii) a single sheet with a vertical extent of a few meters (Fig. 7); (iii) a turbulent layer with a thickness of about 8 m (Fig. 8). As above, we call an altitude region a "sheet" if there is a steep gradient of the temperature and/or specific humidity and if the temperature and/or humidity change does not change its sign within that region. We call an altitude region a (turbulent) layer if the fluctuations of temperature and/or specific humidity within that region change their sign and dominate over the temperature and/or humidity changes due to the respective mean gradient within that region. See also Deaubies and Gregg (1981, 541), who point out that the idealized "sheet-and-layer model" is not necessarily physically correct.

b. Sheets and turbulent layers—Richardson numbers and Reynolds numbers

The magnitude of vertical gradients of velocity or of passive scalars has upper limits because of turbulent or molecular diffusion. A stratified shear flow can become dynamically unstable (Kelvin–Helmholtz instability) if the Richardson number Ri is smaller than a certain critical Richardson number Ri_c , the classical value of which is 0.25. It is known that Ri to be smaller than 0.25 everywhere in the flow is a *necessary* condition for a stratified flow to become dynamically unstable (see, e.g.,

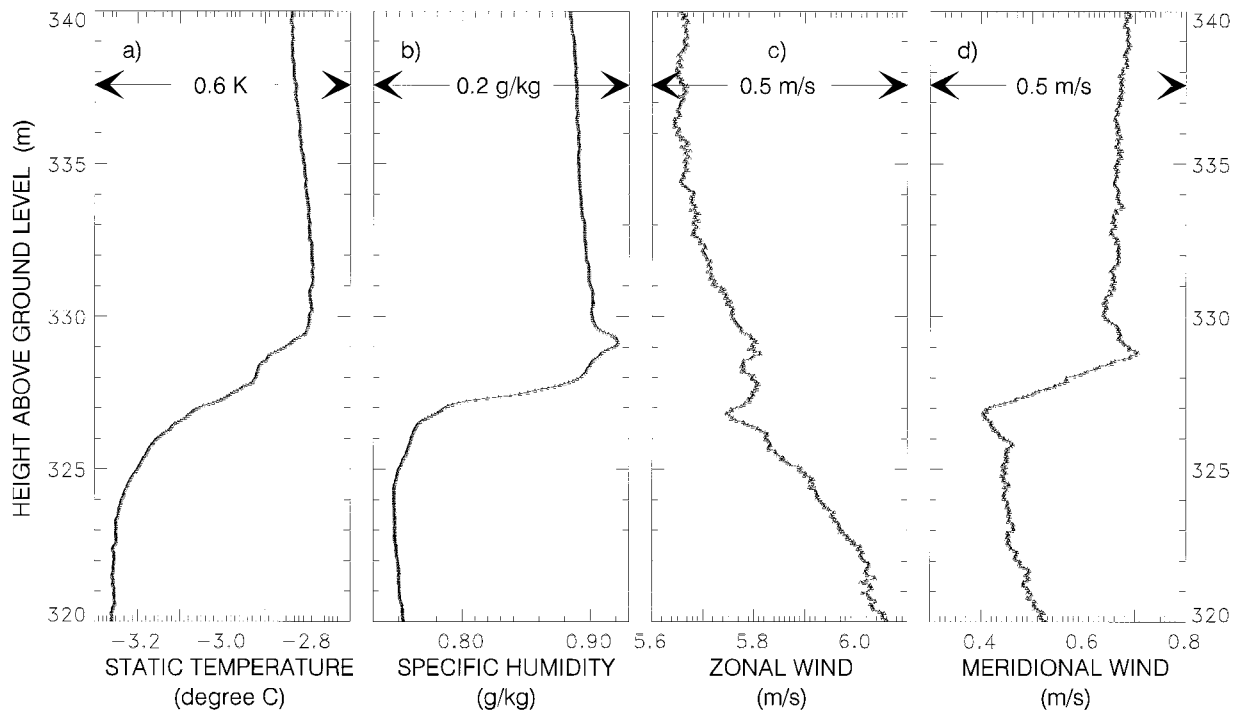


FIG. 7. A sheet observed between 327 m and 329 m AGL observed during leg S7. The figure shows vertical profiles of (a) temperature, (b) specific humidity, (c) zonal wind, and (d) of the meridional wind. Note the increase of the specific humidity q by more than 10% within 1 m.

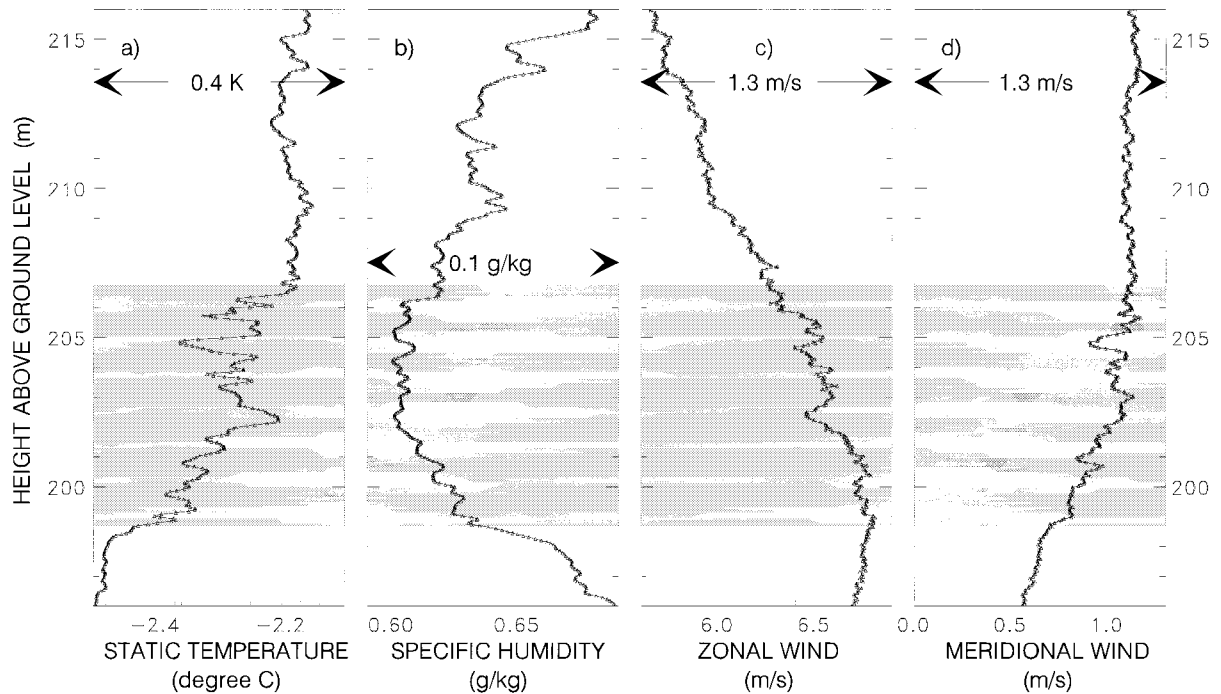


FIG. 8. An 8-m-thick turbulent layer embedded between two submeter sheets at 199 m and at 207 m AGL, respectively, observed during leg S2. Vertical profiles of the same quantities as in Figs. 6 and 7.

Drazin and Reid 1981, 327). During the development and the decay of KHI, there are various stages of billow, sheet, and layer formation (see, e.g., Woods 1969; Browning and Watkins 1970).

The Richardson number for a layer is defined as follows:

$$\text{Ri} = \frac{g \frac{\Delta T}{\Delta z} + \Gamma}{\frac{T \Delta u^2 + \Delta v^2}{\Delta z^2}}, \quad (1)$$

where $g = 9.81 \text{ m s}^{-2}$ is the acceleration due to gravity, and $\Gamma = 9.8 \times 10^{-3} \text{ K m}^{-1}$ is the adiabatic lapse rate.

The turbulent layer shown in Fig. 8 has a thickness of about $\Delta z = 8 \text{ m}$ and is embedded between two thin sheets. The observed profile shown in Fig. 8 is very similar to model profiles suggested by other researchers in order to explain the near-zenith aspect sensitivity of clear-air radar echoes at VHF frequencies; see, for example, Fig. 1 in Lesicar and Hocking (1992) and their references to the earlier literature. To our knowledge the profile shown in Fig. 8 is the first directly observed tropospheric profile of a turbulent layer with a thickness of less than 10 m confined between two submeter sheets.

The temperature difference between the upper and lower boundary of the layer is $\Delta T = 0.15 \text{ K}$, and the changes of the zonal and meridional wind across the layer amount to $\Delta u = -0.4 \text{ m s}^{-1}$ and $\Delta v = 0.3 \text{ m s}^{-1}$, respectively. The absolute temperature of the layer is $T = 271 \text{ K}$. Inserting these values into Eq. (1) leads to $\text{Ri} = 0.26$. This is close to 0.25, which is in line with earlier observations of turbulent layers (Browning et al. 1970; Gossard et al. 1985). The Reynolds number for a layer may be defined as follows:

$$\text{Re} = \frac{\sqrt{\Delta u^2 + \Delta v^2} \Delta z}{\nu}, \quad (2)$$

where ν is the molecular viscosity. At standard conditions, which we assume here for the sake of simplicity, ν amounts to about $1.5 \times 10^{-5} \text{ m}^2 \text{ s}^{-1}$. These values reveal $\text{Re} = 2.7 \times 10^5$ for the 8-m-thick turbulent layer shown in Fig. 8. The large value of Re is consistent with the possibility of fully developed turbulence within the layer.

Now, we come back to the sheet observed during S7 (see Fig. 7). While the temperature profile is rather smooth, the wind profiles, in particular the v -profile (Fig. 7d), show well-marked discontinuities at the altitudes 327 m and 329 m AGL. A closer look at the temperature profile shows that at these altitudes there is a sharpening of the temperature gradient and that the temperature gradient is somewhat smaller in between. We have approximated the observed profiles within this 2-m-wide altitude range by linear profiles and obtained $\Delta z = 2 \text{ m}$, a temperature change $\Delta T = 0.19 \text{ K}$, and wind changes $\Delta u = 0.01 \text{ m s}^{-1}$ and $\Delta v = 0.32 \text{ m s}^{-1}$, respectively. The absolute temperature of the layer is T

$= 270 \text{ K}$. These values lead to $\text{Ri} = 0.15$ and to $\text{Re} = 4.3 \times 10^4$. That is, this thin layer is dynamically even more unstable than the 8-m-thick layer considered previously. Also Re is sufficiently large for molecular viscosity remaining unimportant and to make fully developed turbulence possible. Nevertheless there is no indication for turbulent mixing in the vertical profiles. Maybe the sheet has been traversed by HELIPOD during the initial phase of KHI. This presumption, however, cannot be tested because there are no data about the temporal development of the sheet. The vertical temperature gradient has its largest value between 327 m and 328 m AGL. It amounts to 0.15 K m^{-1} , corresponding to 15Γ .

It is interesting that temperature gradients of 0.15 K m^{-1} and wind shears of up to 0.26 s^{-1} were also observed in weak warm fronts (e.g., Schulze and Roth 1990; Jacobi et al. 1996).

c. How to distinguish between laminar sheets and turbulent layers?

It is of interest to investigate the lower limits of sheet thicknesses. Consider a temperature profile having an initially (i.e., at the time $t = 0$) very sharp step of width ΔT at an altitude, say, $z = 0$. Assume that the step has been generated by some mechanism the details of which do not matter at the moment. It is known from elementary physics that due to molecular diffusion the steplike temperature profile dissolves with increasing time into a Gaussian error function profile (e.g., Thorpe 1969):

$$\frac{\partial T(z, t)}{\partial z} = \frac{\Delta T}{\sqrt{2\pi} \sigma_s(t)} \exp\left(\frac{-z^2}{2\sigma_s^2(t)}\right), \quad (3)$$

where

$$\sigma_s(t) = \sqrt{2\kappa t} \quad (4)$$

is a measure for the thickness of the sheet. Here κ is the molecular diffusivity of heat, and the ratio of ν and κ is known as the molecular Prandtl number,

$$\text{Pr} = \frac{\nu}{\kappa}. \quad (5)$$

It is known that Pr is about 0.7 for air. The length σ_s is a measure for the sheet's thickness. Equation (3) leads to a simple relation between the temperature step ΔT across the sheet and the temperature gradient $(\partial T/\partial z)_c$ in the center of the sheet:

$$\sigma_s = \frac{\Delta T}{\sqrt{2\pi} \left(\frac{\partial T}{\partial z}\right)_c}. \quad (6)$$

Here ΔT can be easily obtained from observed T profiles. Also $(\partial T/\partial z)_c$ can be determined in a simple manner because $(\partial T/\partial z)_c$ is simultaneously the maximum of the temperature gradient within a sheet. Thus, Eq. (6) is a

useful equation for the determination of σ_s . In the following, we will refer to $2\sigma_s$ as the ‘‘sheet thickness’’ d_s :

$$d_s = 2\sigma_s. \quad (7)$$

Assuming $\kappa = 2.1 \times 10^{-5} \text{ m}^2 \text{ s}^{-1}$ for air at standard conditions, which is a reasonable approximation for the lower troposphere, and assuming that the sheets observed during S1 (Fig. 6) are sufficiently well approximated by the model profile defined in Eq. (3), we obtain 26 cm, 36 cm, and 42 cm for d_s of the three sheets observed at 418 m, 421 m, and 425 m AGL, respectively; see Figs. 5 and 6. For the sheet observed during S7, however, we obtain $d_s = 2.4$ m. Resolving Eq. (4) for t leads to a timescale that may be considered a measure for (an upper limit of) the age of the sheet:

$$t_s = \frac{d_s^2}{8\kappa}. \quad (8)$$

Assuming $\kappa = 2.1 \times 10^{-5} \text{ m}^2 \text{ s}^{-1}$, the thicknesses 26 cm, 36 cm, 42 cm, and 2.4 m correspond to the t_s values 7.5 min, 13 min, 17.5 min, and 9.5 h, respectively. While the first three t_s values are of the order of magnitude that is to be expected for the lifetime of atmospheric Kelvin–Helmholtz billows, the fourth value is by about two orders of magnitude larger. There are three explanations: (a) the thick sheet observed during S7 was not the result of KHI but, rather, is the inversion of a warm front, having a synoptic-scale lifetime (we tend to rule out this possibility, however, because there was no indication for the presence of a warm front in the synoptic material); (b) during the initial phase of the formation of the sheet, there was a turbulent layer in its center before dying out again, giving rise to more efficient diffusion, which flattened the temperature in its center; (c) the central layer within each of the inversions was still turbulent when it was traversed by HELIPOD but the outer scale of the turbulence was too small to allow the turbulence to be resolved in the time series.

Indeed, a closer look at the temperature profiles within the observed four sheets suggests that there is a tiny less stable or even isothermal layer in the center of each sheet, suggesting that the center of each sheet was turbulent during an earlier stage of its development or even still turbulent when it was observed. Note that the two ‘‘subsheets’’ of each of the three sheets observed during S1 (Fig. 6) have thicknesses down to about 10 cm.

In order to decide between the three above-mentioned hypotheses, we will derive first a lower physical limit for the thickness of a turbulent layer and second an equation for the thinnest turbulent layer that can be identified with a given sampling rate of an in situ turbulence sonde.

d. The critical thickness of a turbulent layer

From Eqs. (1) and (2) we derive a critical layer thickness d_c :

$$d_c = \left(\frac{T\nu^2}{gf_\gamma\Gamma} \text{Ri}_c \text{Re}_c^2 \right)^{1/4}, \quad (9)$$

where Ri_c and Re_c are the critical Richardson and Reynolds numbers, respectively, and f_γ is the mean potential temperature gradient across the layer in units of the adiabatic lapse rate Γ :

$$f_\gamma = \frac{\gamma + \Gamma}{\Gamma} = \frac{\frac{\Delta T}{d_c} + \Gamma}{\Gamma}. \quad (10)$$

Assuming $T = 273$ K, $f_\gamma = 1$ (isothermal layer), $\nu = 1.5 \times 10^{-5} \text{ m}^2 \text{ s}^{-1}$ (lower troposphere), $\text{Ri}_c = 0.25$, and $\text{Re}_c = 1000$, we obtain $d_c = 63$ cm. That is, the thinnest isothermal turbulent layer is about 63 cm thick. Note that d_c depends only weakly on f_γ . Even in the case $f_\gamma = 40$, which may be considered the maximum value of atmospheric vertical temperature gradients, the thickness is reduced by only the factor 2.5 in comparison with an isothermal layer. It is interesting that these values for d_c are very close to the thicknesses of the smallest observed sheets or layers (Fig. 6) and also very close to the thickness of an initially infinitely sharp temperature step after about 10 min [see Eq. (7)].

The critical layer thickness can also be stated in terms of the Brunt–Väisälä frequency N or in terms of the Brunt–Väisälä period $T_{\text{BV}} = 2\pi/N$. Inserting

$$N^2 = \frac{g}{T}(\gamma + \Gamma) \quad (11)$$

into Eq. (9) provides

$$d_c = \left(\frac{\nu^2}{N^2} \text{Ri}_c \text{Re}_c^2 \right)^{1/4} = \sqrt{2\pi\nu T_{\text{BV}}} (\text{Ri}_c \text{Re}_c^2)^{1/4}. \quad (12)$$

Note that the layer thickness given by Eq. (12) is very similar to the vertical wavelength λ_z of a viscosity–thermal-conduction wave [Eq. (4) in Hocking et al. (1991, 1287)]:

$$\lambda_z = 2\sqrt{\pi} \sqrt{\nu T_w}, \quad (13)$$

where T_w is the temporal period of the primary wave.

We have introduced three lengths: (a) the thickness d_s of an initially sharp temperature step after the time t_s , (b) the thickness d_c of the thinnest layer that could be turbulent, and (c) the wavelength λ_z of a viscosity wave. All these three lengths are, apart from a numerical factor, equal to the square root of the product of the molecular viscosity ν and a characteristic timescale. The timescales are the (maximum) age of a laminar sheet with a given thickness, the Brunt–Väisälä period, and the period of a primary gravity wave, respectively.

A similar intrinsic relationship between mesoscale and molecular time and length scales was pointed out by Muschinski (1994), who put forward an atomistic interpretation of the Brunt–Väisälä period for the lower boundary of the exosphere.

Because d_c is proportional to the square root of ν it is to be expected that d_c increases like $\exp(+z/2H)$ with the altitude z , where H is the scale height of the atmosphere. That is, the thinnest lower-tropospheric sheets and layers are expected thinner than the thinnest upper-tropospheric or stratospheric turbulent layers. This expectation, however, is not in line with the layer-thickness statistics presented by Dalaudier et al. (1994, their Table 1). Maybe the altitude dependence of ν is not the dominating effect that determines the variation of the sheet and layer thickness with the altitude.

e. Observability of thin turbulent layers using rapidly moving in situ sondes

Figure 8 shows the vertical profiles of T , q , u , and v as observed by HELIPOD when it traversed an 8-m-thick turbulent layer in the altitude range between 199 m and 207 m AGL during S7. As mentioned above, all four profiles show a significantly enhanced small-scale variability within the layer in comparison with its upper and lower environment. The structures near the middle of the layer have apparent vertical extensions of somewhat less than 1 m. At this point it is important to note that the vertical structure shown in Fig. 8 is *apparent* because HELIPOD crossed the layer at a downward velocity v_d of about 5 m s⁻¹ and a forward velocity v_f of about 40 m s⁻¹. That is, HELIPOD collected data along a straight line that has a slope of $v_d/v_f \approx 1/8$. While HELIPOD moved downward by somewhat less than 1 m, simultaneously it moved forward by somewhat less than 8 m. Thus, the 1-m structures that appear in the “vertical” profile shown in Fig. 8 are in fact 8-m structures along the flight path. It is to be expected that the largest turbulent eddies in a turbulent layer of a width d have a diameter close to d itself; that is, the size of the apparent structures of somewhat less than 1 m in Fig. 8 coincide well with the observed layer thickness of 8 m. A maximum eddy diameter d corresponds to the wavelength:

$$\lambda_{\max} = 2d, \quad (14)$$

or to the wavenumber $2\pi/(2d)$ (e.g., Heisenberg 1948, 635; Muschinski and Roth 1993, 338; Muschinski 1996b). According to the sampling theorem, the minimum sampling rate f_{\min} necessary to unambiguously sample structures of the wavelength $2d$ using a measuring device moving through space with a “sensor velocity” v_s is given by

$$f_{\min} = 2\frac{v_s}{2d} = \frac{v_s}{d}. \quad (15)$$

For example, to resolve the largest eddies in a 1-m-wide turbulent layer for a sensor velocity of 50 m s⁻¹ a sampling rate of at least 50 Hz is necessary. On the other hand, one obtains an equation for the lower limit of the thickness d_{\min} of a layer the large eddies within which

are to be resolved for a given sampling rate n and a given sensor velocity v_s :

$$d_{\min} = \frac{v_s}{f}. \quad (16)$$

During the experiment described above, the sampling rate was 100 Hz, and HELIPOD moved with a sensor velocity of about 40 m s⁻¹. This leads to a “resolvable layer thickness” of 40 cm. In other words: it is not possible to decide directly from the data whether the thin “sheets” shown in Fig. 6 are laminar or turbulent.

f. Implications for clear-air radar scatter and reflection

Since the development of the first atmospheric radars, there has been a continuous debate on whether fully developed turbulence or thin laminae are dominating in causing clear-air radar echoes. The discussion is most controversial concerning the reflection–scatter mechanisms at VHF echoes from the stably stratified atmosphere. Generally, the near-zenith echo-intensity maximum observed at VHF frequencies (Röttger and Liu 1978; Gage and Green 1978) is attributed to Fresnel-scatter from thin laminae in the stably stratified free atmosphere (e.g. Röttger 1980; Gage et al. 1981; Doviak and Zrnić 1984; Gage 1990; Luce et al. 1995), while it is believed that at oblique beam directions Bragg-scatter from refractive-index irregularities due to Kolmogorovian small-scale turbulence is the most important echoing mechanism (VanZandt et al. 1978; Doviak and Zrnić 1984; Gage 1990; Muschinski 1997; Luce et al. 1996). Röttger and Liu (1978) found larger correlation times for vertical-beam echoes than for tilted-beam echoes, confirming the nonturbulent nature of vertical-beam echoes at VHF frequencies. The occasional relevance of specular reflection from a single sheet within one range gate (Fresnel-reflection) has been further corroborated by Sheen et al.’s (1985) study of VHF radar signal statistics. The attribute “Fresnel” stands for transverse coherence and was coined by S. Bowhill [see, e.g., the acknowledgments in Gage et al. (1981)].

Because of the lack of obvious near-zenith aspect sensitivity of clear-air echoes at UHF frequencies, nowadays specular UHF echoes from laminar sheets are generally considered negligible (Doviak 1997, personal communication). On the other hand, during the early days of radar meteorology there was an intense debate on the possible importance of specular UHF echoes from very thin laminae [e.g., Atlas (1960a), Atlas (1960b), Atlas (1965); see also the footnote on p. 535 in Gage (1990)]. The observations by Metcalf and Atlas (1973) support the presumption of the possible importance of specular UHF echoes under certain conditions; see also Gossard (1990, 488 ff.).

6. Summary, conclusions, and outlook

We have presented and discussed high-resolution in situ observations of sheets and layers in the Arctic lower free troposphere. The measurements were carried out on 13 October 1995 during a high pressure period, using the new helicopter-borne multisensoral turbulence sonde HELIPOD.

We have presented first in situ evidence of coexisting free-tropospheric temperature and humidity sheets having thicknesses down to a few decimeters. We have observed vertical temperature gradients of up to about 17Γ , where Γ is the adiabatic lapse rate, in close agreement with high-resolution balloon-sonde observations by Dalaudier et al. (1994). The magnitudes of the temperature variations across the sheets range from a few K to about 0.3 K. Moreover, we have presented the first directly observed tropospheric temperature, humidity, and wind velocity profiles of a single turbulent layer with a thickness of less than 10 m confined between two submeter sheets.

We have shown by simple theoretical reasoning that sheet thicknesses, regardless of whether they are the remnants of Kelvin–Helmholtz instability or attributed to viscosity/thermal-conduction waves, should amount (apart from a numerical factor) to the square root of the product of molecular kinematic viscosity and a timescale that characterizes the age of a laminar sheet, the lifetime of a Kelvin–Helmholtz billow, or the period of a primary gravity wave. Assuming a timescale of 10 min leads to an estimated sheet thickness of about 10 cm for the lower troposphere, which is in good agreement with our observations.

Further analysis of the present dataset and of measurements to be made in the future is necessary to decide to which extent our findings are representative for the stably stratified free troposphere in general and to which extent such structures are important for clear-air radar echoes in the VHF and UHF regime.

Acknowledgments. The financial funding for the construction of HELIPOD was provided by the Bundesministerium für Bildung, Wissenschaft, Forschung und Technologie (BMBF Contract 07 KFT 74). The operation of HELIPOD during the ARK-XI/2 campaign was funded by the Deutsche Forschungsgemeinschaft (DFG Contract IIC7-Ro395/12-1).

REFERENCES

- Atlas, D., 1960a: Possible key to the dilemma of meteorological “angel” echoes. *J. Meteor.*, **17**, 95–103.
- , 1960b: Radar detection of the sea breeze. *J. Meteor.*, **17**, 244–258.
- , 1965: Angels in focus. *Radio Sci.*, **69D**, 871–875.
- , J. I. Metcalf, J. H. Richter, and E. E. Gossard, 1970: The birth of “CAT” and microscale turbulence. *J. Atmos. Sci.*, **27**, 903–913.
- Blanc, T. V., W. J. Plant, and W. C. Keller, 1989: The Naval Research Laboratory’s air–sea interaction blimp experiment. *Bull. Amer. Meteor. Soc.*, **70**, 354–365.
- Browning, K. A., and C. D. Watkins, 1970: Observations of clear air turbulence by high power radar. *Nature*, **227**, 260–263.
- , T. W. Harrold, and J. R. Starr, 1970: Richardson number limited shear zones in the free atmosphere. *Quart. J. Roy. Meteor. Soc.*, **96**, 40–49.
- Büchler, R., 1993: Untersuchungen zum aerodynamischen Störfeld an einer Hubschrauberschleppsonde. MS thesis 93-4D, Institute for Flight Mechanics, Technical University of Braunschweig, Germany, 99 pp. + appendix. [Available from Institute for Flight Mechanics, Technical University of Braunschweig, Schleinitzstraße 20, 38106 Braunschweig, Germany.]
- Chilson, P. B., A. Muschinski, and G. Schmidt, 1997: First observations of Kelvin–Helmholtz billows in an upper-level jet stream using VHF frequency domain interferometry. *Radio Sci.*, **32**, 1149–1160.
- Dalaudier, F., C. Sidi, M. Crochet, and J. Vernin, 1994: Direct evidence of “sheets” in the atmospheric temperature field. *J. Atmos. Sci.*, **51**, 237–248.
- Desaubies, Y., and M. C. Gregg, 1981: Reversible and irreversible finestructure. *J. Phys. Oceanogr.*, **11**, 541–556.
- Doviak, R. J., and D. S. Zrnić, 1984: Reflection and scatter formula for anisotropically turbulent air. *Radio Sci.*, **19**, 325–336.
- Drazin, P. G., and W. H. Reid, 1981: *Hydrodynamic Stability*. Cambridge University Press, 525 pp.
- Eaton, F. D., S. A. McLaughlin, and J. R. Hines, 1995: A new frequency-modulated continuous wave radar for studying planetary boundary layer morphology. *Radio Sci.*, **30**, 75–88.
- Fritts, D. C., and P. K. Rastogi, 1985: Convective and dynamical instabilities due to gravity wave motions in the lower and middle atmosphere: Theory and observations. *Radio Sci.*, **20**, 1247–1277.
- Gage, K. S., 1990: Radar observations in the free atmosphere: Structure and dynamics. *Radar in Meteorology*, D. Atlas, Ed., Amer. Meteor. Soc., 534–565.
- , and J. L. Green, 1978: Evidence for specular reflection from monostatic VHF radar observations of the stratosphere. *Radio Sci.*, **13**, 991–1001.
- , B. B. Balsley, and J. L. Green, 1981: Fresnel scattering model for the specular echoes observed by VHF radar. *Radio Sci.*, **16**, 1447–1453.
- Gossard, E. E., 1990: Radar research on the atmospheric boundary layer. *Radar in Meteorology*, D. Atlas, Ed., Amer. Meteor. Soc., 477–527.
- , and J. H. Richter, 1970: The shape of internal waves of finite amplitude from high-resolution radar sounding of the lower atmosphere. *J. Atmos. Sci.*, **27**, 971–973.
- , D. R. Jensen, and J. H. Richter, 1971: An analytical study of tropospheric structure as seen by high-resolution radar. *J. Atmos. Sci.*, **28**, 794–807.
- , J. H. Richter, and D. R. Jensen, 1973: Effect of wind shear on atmospheric wave instabilities revealed by FM/CW radar observations. *Bound.-Layer Meteor.*, **4**, 113–131.
- , J. E. Gaynor, R. J. Zamora, and W. D. Neff, 1985: Finestructure of elevated stable layers observed by sounder and in situ tower sensors. *J. Atmos. Sci.*, **42**, 2156–2169.
- Heisenberg, W., 1948: Zur statistischen Theorie der Turbulenz. *Z. Phys.*, **124**, 628–657.
- Hicks, J. J., and J. K. Angell, 1968: Radar observations of breaking gravitational waves in the visually clear atmosphere. *J. Appl. Meteor.*, **7**, 114–121.
- Hocking, W. K., S. Fukao, M. Yamamoto, T. Tsuda, and S. Kato, 1991: Viscosity waves and thermal-conduction waves as a cause of “specular” reflectors in radar studies of the atmosphere. *Radio Sci.*, **26**, 1281–1303.
- Hooke, W. H., and R. M. Jones, 1986: Dissipative waves excited by gravity-wave encounters with the stably stratified planetary boundary layer. *J. Atmos. Sci.*, **43**, 2048–2060.
- Imberger, J., and G. N. Ivey, 1991: On the nature of turbulence in a

- stratified fluid. Part II: Application to lakes. *J. Phys. Oceanogr.*, **21**, 659–680.
- Jacobi, C., A. H. Siemer, and R. Roth, 1996: On wind shear at fronts and inversions. *Meteor. Atmos. Phys.*, **59**, 235–243.
- Klostermeyer, J., and R. Ruster, 1980: Radar observations and a model computation of a jet stream-generated Kelvin-Helmholtz instability. *J. Geophys. Res.*, **85**, 2841–2846.
- Krause, G., 1996: The expedition ARK-XI/2 of RV *Polarstern* in 1995. Reports on Polar Research, No. 197, Alfred Wegener Institute for Polar and Marine Research, Bremerhaven, Germany, 65 pp. [Available from Alfred Wegener Institute for Polar and Marine Research, Columbusstraße, 27568 Bremerhaven, Germany.]
- Lesicar, D., and W. K. Hocking, 1992: Studies of seasonal behaviour of the shape of mesospheric scatterers using a 1.98 MHz radar. *J. Atmos. Terr. Phys.*, **54**, 295–309.
- Luce, H., M. Crochet, F. Dalaudier, and C. Sidi, 1995: Interpretation of VHF ST radar vertical echoes from in situ temperature sheet observations. *Radio Sci.*, **30**, 1003–1025.
- , F. Dalaudier, M. Crochet, and C. Sidi, 1996: Direct comparison between in situ and VHF oblique radar measurements of refractive index spectra: A new successful attempt. *Radio Sci.*, **31**, 1487–1500.
- Metcalf, J. I., and D. Atlas, 1973: Microscale ordered motions and atmospheric structure associated with thin echo layers in stably stratified zones. *Bound.-Layer Meteor.*, **4**, 7–35.
- Muschinski, A., 1994: Eine atomistische Deutung der Brunt-Väisälä-Periode. *Meteor. Z. N. F.*, **3**, 94–95.
- , 1996a: Possible effect of Kelvin-Helmholtz instability on VHF radar observations of the mean vertical wind. *J. Appl. Meteor.*, **35**, 2210–2217.
- , 1996b: A similarity theory of locally homogeneous and isotropic turbulence generated by a Smagorinsky-type LES. *J. Fluid Mech.*, **325**, 239–260.
- , 1997: Turbulence and gravity waves in the vicinity of a mid-tropospheric warmfront—A comparative case study using VHF echo-intensity measurements and rawinsonde data. *Radio Sci.*, **32**, 1161–1178.
- , and R. Roth, 1993: A local interpretation of Heisenberg's transfer theory. *Beitr. Phys. Atmos.*, **66**, 335–346.
- Nastrom, G. D., T. E. VanZandt, W. L. Clark, J. M. Warnock, J. L. Green, and K. S. Gage, 1990: Diagnosis of a downward bias in the vertical motions seen by VHF clear-air Doppler radars. *Eos, Trans. Amer. Geophys. Union*, **71**, 28.
- Pitteway, M. L. V., and C. O. Hines, 1963: The viscous damping of atmospheric gravity waves. *Can. J. Phys.*, **41**, 1935–1948.
- Posmentier, E. S., 1977: The generation of salinity finestructure by vertical diffusion. *J. Phys. Oceanogr.*, **7**, 298–300.
- Röttger, J., 1980: Reflection and scattering of VHF radar signals from atmospheric refractivity structures. *Radio Sci.*, **15**, 259–276.
- , and C.-H. Liu, 1978: Partial reflection and scattering of VHF radar signals from the clear atmosphere. *Geophys. Res. Lett.*, **5**, 357–360.
- Schulze, O., and R. Roth, 1990: Flugsicherheitsrelevante Scherungen an einer Warmfront. *Meteor. Rundsch.*, **43**, 156–160.
- Schürmann, M., and C. Wode, 1996: HELIPOD—A turbulence measurement system for meteorological research. *Proc. Second Int. Airborne Remote Sensing Conf. and Exhibition*, San Francisco, CA, Environmental Research Institute of Michigan, 451–452.
- Sheen, D. R., C. H. Liu, and J. Röttger, 1985: A study of signal statistics of VHF radar echoes from clear air. *J. Atmos. Terr. Phys.*, **47**, 675–684.
- Thorpe, S. A., 1969: Experiments on the stability of stratified shear flows. *Radio Sci.*, **4**, 1327–1331.
- VanZandt, T. E., J. L. Green, K. S. Gage, and W. L. Clark, 1978: Vertical profiles of refractivity turbulence structure constant: Comparison of observations by the Sunset Radar with a new theoretical model. *Radio Sci.*, **13**, 819–829.
- Vörsmann, P., 1990: METEOPD—An airborne system for measurements of mean wind, turbulence, and other meteorological parameters. Report, Aerodata Flugmesstechnik GmbH, Braunschweig, Germany, 17 pp. [Available from Aerodata Flugmeßtechnik GmbH, Hermann-Blenk-Straße 36, 38108 Braunschweig, Germany.]
- WCRP-72, 1992: Scientific concept of the Arctic Climate System Study (ACSYS). WMO/TD-No. 486, 89 pp.
- WCRP-85, 1994: Arctic Climate System Study (ACSYS)—Initial implementation plan. WMO/TD-No. 627, 66 pp.
- Wode, C., and R. Roth, 1996: HELIPOD—Ein hubschraubergestütztes meteorologisches Meßsystem. Abschlußbericht zu dem BMFT-Fördervorhaben 07 KFT 74, Institute for Meteorology and Climatology, University of Hannover, Hannover, Germany, 145 pp. [Available from Institute for Meteorology and Climatology, University of Hannover, Herrenhäuser Straße 2, 30419 Hannover, Germany.]
- , and C. Wamser, 1996: Turbulence measurements. The expedition ARK-XI/2 of RV *Polarstern* in 1995. Reports on Polar Research, No. 197, Alfred Wegener Institute for Polar and Marine Research, Bremerhaven, Germany, 10–16. [Available from Alfred Wegener Institute for Polar and Marine Research, Columbusstraße, 27568 Bremerhaven, Germany.]
- , R. Roth, and M. Schürmann, 1996: The helicopter-borne sensor package HELIPOD—Features and capabilities of a new turbulence measurement system for meteorological research. *Proc. Second Int. Airborne Remote Sensing Conference and Exhibition*, San Francisco, CA, Environmental Research Institute of Michigan, 483–491.
- Woodman, R. F., and Y. Y.-H. Chu, 1989: Aspect sensitivity measurements of VHF backscatter made with the Chung-Li radar: Plausible mechanisms. *Radio Sci.*, **24**, 113–125.
- Woods, J. D., 1968: Wave-induced shear instability in the summer thermocline. *J. Fluid Mech.*, **32**, 791–800.
- , 1969: On Richardson's number as a criterion for laminar-turbulent-laminar transition in the ocean and atmosphere. *Radio Sci.*, **4**, 1289–1298.